NeuroImage 248 (2022) 118862

Contents lists available at ScienceDirect

NeuroImage

journal homepage: www.elsevier.com/locate/neuroimage

Robotically-induced hallucination triggers subtle changes in brain network transitions

Herberto Dhanis[a,b,c,d], Eva Blondiaux[a,b], Thomas Bolton[c,d], Nathan Faivre[a,b,e], Giulio Rognini[a,b], Dimitri Van De Ville[a,c,d,1,*], Olaf Blanke[a,b,f,1,*]

[a] Center for Neuroprosthetics, Ecole Polytechnique Fédérale de Lausanne, EPFL, Geneva, Switzerland
[b] Brain Mind Institute, Faculty of Life Sciences, Ecole Polytechnique Fédérale de Lausanne, Lausanne, Switzerland
[c] Institute of Bioengineering, Ecole Polytechnique Fédérale de Lausanne, Lausanne Switzerland
[d] Department of Radiology and Medical Informatics, University of Geneva, Geneva Switzerland
[e] University. Grenoble Alpes, University Savoie Mont Blanc, CNRS, LPNC, 38000 Grenoble, France
[f] Department of Clinical Neurosciences, University Hospital of Geneva, Geneva, Switzerland

ARTICLE INFO

Keywords:
Presence Hallucination
Dynamic functional connectivity
Co-activation pattern analysis
Network interactions
Psychosis
Robotics

ABSTRACT

The perception that someone is nearby, although nobody can be seen or heard, is called presence hallucination (PH). Being a frequent hallucination in patients with Parkinson's disease, it has been argued to be indicative of a more severe and rapidly advancing form of the disease, associated with psychosis and cognitive decline. PH may also occur in healthy individuals and has recently been experimentally induced, in a controlled manner during fMRI, using MR-compatible robotics and sensorimotor stimulation. Previous neuroimaging correlates of such robot-induced PH, based on conventional time-averaged fMRI analysis, identified altered activity in the posterior superior temporal sulcus and inferior frontal gyrus in healthy individuals. However, no link with the strength of the robot-induced PH was observed, and such activations were also associated with other sensations induced by robotic stimulation. Here we leverage recent advances in dynamic functional connectivity, which have been applied to different psychiatric conditions, to decompose fMRI data during PH-induction into a set of co-activation patterns that are tracked over time, as to characterize their occupancies, durations, and transitions. Our results reveal that, when PH is induced, the identified brain patterns significantly and selectively increase their transition probabilities towards a specific brain pattern, centred on the posterior superior temporal sulcus, angular gyrus, dorso-lateral prefrontal cortex, and middle prefrontal cortex. This change is not observed in any other control conditions, nor is it observed in association with other sensations induced by robotic stimulation. The present findings describe the neural mechanisms of PH in healthy individuals and identify a specific disruption of the dynamics of network interactions, extending previously reported network dysfunctions in psychotic patients with hallucinations to an induced robot-controlled specific hallucination in healthy individuals.

1. Introduction

The sense of presence or presence hallucination (PH) is the sensation of feeling another person close by when in fact no one is actually there (James, 1902). It has been described as an incomplete hallucination, which although vividly perceived, cannot be attributed to any of the usual "sensible ways", such as visual and auditory perception (James, 1902; Jaspers, 1913). PH has been reported in a variety of medical disorders ranging from stroke (Blanke et al., 2003) to epilepsy (Blanke et al., 2014), brain stimulation during invasive presurgical evaluations (Arzy et al., 2006a), and schizophrenia (Jaspers, 1913). PH is also one of the most frequent hallucinations in Parkinson's Disease (Diederich et al., 2009; Fénelon et al., 2011) and has also been reported by healthy individuals in extreme situations (e.g., Messner, 2016).

Clinical evidence suggests that altered processing of bodily and sensorimotor signals is an important mechanism in PH, given the 'sharing' of posture, position, and movement between the patient and the 'presence', as well as the association of PH with sensorimotor deficits (Brugger et al., 1996, 1997; Blanke et al., 2008). Although the paroxysmal and short-lasting characteristics of PH made it difficult to study this hallucination, Arzy et al. (2006a) demonstrated that the PH can be induced repeatedly and in a controlled fashion through electrical brain

* Corresponding authors.
E-mail addresses: dimitri.vandeville@epfl.ch (D. Van De Ville), olaf.blanke@epfl.ch (O. Blanke).
[1] Both authors contributed equally.

https://doi.org/10.1016/j.neuroimage.2021.118862.
Received 8 March 2021; Received in revised form 19 November 2021; Accepted 23 December 2021
Available online 28 December 2021.

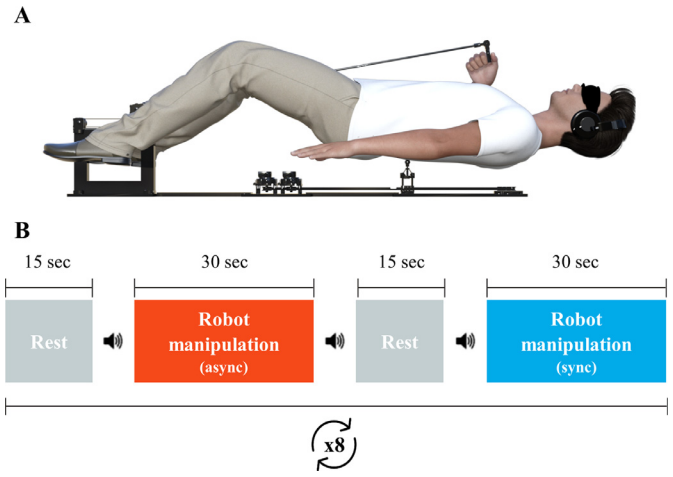

Fig. 1. Robotic system and experimental paradigm
(A) MR-compatible robotic system used to induce the PH in healthy individuals. The robotic system is composed of a front part, which has a manipulator stick slide on a rail, and allows the participants to move in the x (bottom and up) and z (up and down) directions. These movements are then transmitted to a back robot that is confined below an MR-compatible platform. In the present experiment the back robot mimics the movements of the front part of the robotic system either in real-time, or with a delay of 500 milliseconds. **(B)** During the experiment participants perform two runs, each with sixteen 30 second blocks of robotic manipulation, interleaved with 15 s of rest. The blocks of robotic manipulation are performed in the synchronous condition, where movements with the front robot are reproduced in real-time by the back robot, or in the asynchronous condition, where movements with the back robot are reproduced by the back robot with a delay of 500 milliseconds. Blocks of the same type do not appear more than twice in a row. Auditory cues passed on to the participant through headphones, mark the beginning and ending of each block. (Adapted from Bernasconi et al., 2021).

stimulation of the temporo-parietal junction (TPJ), a major integration hub for multisensory and sensorimotor bodily signals (Matsuhashi et al., 2004; Arzy et al., 2006b; Blanke, 2012).

Based on these clinical data, Blanke et al. (2014) showed that a robotic setup is capable of inducing a sensation comparable to PH. In this setup, participants actuate two interconnected robots that allow to modulate the intensity of robotically induced PH by changing the delay between the movements of the participant and the tactile feedback on the back of the participant. Stronger PH occurs when a delay between movements and feedback is inserted (asynchronous condition; Fig. 1), rather than when it is not (synchronous condition). Using MR-compatible robotics and fMRI in healthy participants, an extended network was identified to be associated with PH (Bernasconi et al., 2021). Moreover, these authors used lesion network mapping analysis from neurological patients reporting symptomatic PH to further corroborate the PH network, leading to three areas that overlapped with the regions revealed by fMRI during robot-induced PH: the posterior part of the middle temporal gyrus and superior temporal sulcus (pSTS), ventral premotor cortex (vPMC), and the inferior frontal gyrus (IFG) (Bernasconi et al., 2021). From these three regions, only the pSTS and IFG differed in their activity between the asynchronous versus synchronous condition and were further considered for the present study.

Despite the implication of pSTS and IFG regions in the difference between asynchronous versus synchronous condition, their activities did not correlate with the intensity of the robot-induced PH. In addition, concomitant to the induction of the PH in the asynchronous condition, robotic stimulation also induced certain passivity experiences (PE; i.e., the sensation that someone else is touching your body; (Mlakar et al., 1994), with most participants that experienced PH reporting it in unison with PE, while others that did not experience PH still reporting PE. Considering that clinical observations have highlighted the paroxysmal nature and short duration of PH (Blanke et al., 2008; Fénelon et al., 2011), we hypothesize that the temporal dynamics of the PH's neural underpinnings might share these aspects, and hence could be revealed with methods detecting dynamic changes in brain activity.

In the present study, we set to identify the neural mechanisms of the PH in more detail. We focus particularly on studying the temporal dynamics and more subtle changes in brain activity that might underlie PH. To do so, we investigated fMRI BOLD signal during the robotic sensorimotor task, used to induce the PH (Bernasconi et al., 2021), and applied recently established dynamic functional connectivity (dFC) methods that can capture whole-brain network fluctuations in short time ranges (Hutchison et al., 2013; Preti et al., 2017) and that have shown promising results in the study and differentiation of psychiatric conditions (Damaraju et al., 2014; Rashid et al., 2014; Bolton et al., 2020a). Specifically, we apply Co-Activation Patterns (CAPs; Liu and Duyn, 2013) analysis to investigate the dynamically occurring and spatially distributed activity patterns that reflect functional networks associated with the induction of PH and of PE. CAP analysis is based on the assumption that when the BOLD signal is high in relevant seed regions (Tagliazucchi et al., 2011, 2012), different CAPs are expressed at different moments in time (Liu and Duyn, 2013). As seeds, we chose the two key regions (pSTS, IFG) that were associated with both the PH-inducing condition in healthy people and the network in neurological patients with PH (Bernasconi et al., 2021). The CAPs related to these seeds were characterized by their occupancy, average duration, and transition probabilities (Chen et al., 2015; Bolton et al., 2020b), and compared across the two experimental conditions and rest, as well as between different intensities of PH and PE.

Based on our proposition for a short-lived brain mechanism for PH, we hypothesized that its neural correlates would consist in a temporary dominance of certain CAPs (e.g. increased occupancy, average duration, or a shift in transition probabilities favouring one or more CAPs), a process comparable to network intrusions following the disengagement of intrinsic networks (i.e. decreased anticorrelation between intrinsic and sensory networks) that have been observed in other types of hallucinations (Jardri et al., 2013; Shine et al., 2015) and potentially related to neural processes described for PH and other hallucinations in Parkinson's disease (Bejr-kasem et al., 2018; Lenka et al., 2019). We furthermore hypothesized that the neural mechanisms of PH might extend from the seed regions (pSTS, IFG) to frontal and parietal regions, in particular the inferior parietal lobule (IPL), as this region has been involved in neurological patients with PH (Blanke et al., 2014) and to dorsolateral prefrontal cortex (dlPFC), as IPL and dlPFC have been implicated in comparable sensorimotor tasks which investigated the sense of agency (Farrer and Frith, 2002; Farrer et al., 2008).

2. Materials and methods

The present study performed dFC analysis on the data from Bernasconi et al. (2021). The following sections will summarise the participants included, and the experimental design used in that study, as well as the analysis and methodologies employed in the present study.

2.1. Participants

25 healthy individuals (10 females) with a mean age of 24.68 (± 3.70, range 18–32) years old took part in the PH-induction experiment (study 2.1 in Bernasconi et al., 2021). Every participant was right-handed as assessed by the Edinburgh Handedness Inventory (Oldfield, 1971). All participants gave their informed consent prior to the start of the experiment, following the Declaration of Helsinki, and the study was approved by the local ethics committee of the Canton of Genève, Switzerland.

2.2. Experimental paradigm

Throughout the experiment, participants were blindfolded with an eye masque and wore both ear protection and headphones, in an effort to maximally isolate them from the surroundings. Laying on top of a special platform-bed, that concealed the back part of the robotic system used to induce PH, participants could manipulate a lever attached to the front part of the robotic system (Fig. 1A). The robot itself, composed of a front and back part, allows its users to provide tactile feedback on their own backs. This is achieved by moving the front part of the system with a lever, which controls the back part of the robot that provides tactile feedback on the participant's back. A conflict in the spatial domain is hence always present, with the movements performed in the front space being perceived immediately on the back space (synchronous condition). A second conflict can be introduced in the temporal domain, by delaying the feedback received on the back (asynchronous condition). In the asynchronous condition where these two conflicts are combined, the sensation of having someone behind you (PH), and the sensation that someone else producing is your actions (PE), can be elicited in healthy individuals (Blanke et al., 2014).

The task itself consisted of 16 blocks of 30 s of robot manipulation, interleaved by blocks of 15 s of rest (Fig. 1B). Two conditions were assessed: the synchronous condition in which the movements performed by the participants with the front part of the system were synchronously reproduced onto their backs, and the asynchronous condition where a delay of 500 ms was introduced between the performed movement and the tactile feedback. The conditions were presented randomly to the participants, with no same condition being delivered more than twice in a row. In total, each participant performed two runs, with a total duration of 25 min.

At the end of the scanning session, participants performed 30 s of robotic manipulation for each condition (i.e., synchronous and asynchronous) in a counterbalanced fashion. After each condition, participants answered a questionnaire assessing their subjective experience during the robotic stimulation (7-point Likert scale, see Supplementary Table S1). The questionnaire included questions such as, "I felt as if I was touching my body", to assess self-touch impressions, "I felt as if someone else was touching my body", to assess PE, and "I felt as if someone was behind me" to assess PH. For each participant we computed the strength of the induced sensations, respectively for each questionnaire item, as the difference between the score in the asynchronous and synchronous conditions. A positive score reflects an induced sensation that is stronger in the asynchronous condition, whereas a negative score indicates a stronger sensation in the synchronous condition.

2.3. MRI data acquisition

Functional image acquisitions were performed at the MRI facility of the Campus Biotech (Geneva, Switzerland), with a Siemens MAGNETON Prisma 3T scanner, and using a 64-channel head-and-neck coil. For the sensorimotor task, echo-planar sequences were used (EPI, TR = 2.5 s, TE = 30 ms, with a flip angle of 90°, GRAPPA = 2), with a resolution of 2.5 × 2.5 mm, and a slice thickness of 2.5 mm (no gap, 43 slices). Anatomical images were acquired with T1-weighted MPRAGE sequences (192 slices, FOV = 240 mm, TR = 2.3 s, TE = 2.32 ms).

2.4. Dynamic functional connectivity analysis through co-activation patterns

CAPs analysis is based on point process analysis (Tagliazucchi et al., 2012) and temporal clustering (Liu and Duyn, 2013). In particular, given the activity time course of one or more seed regions, different dynamically occurring network configurations that co-activate with these seeds are extracted. For the present implementation, we built upon the Tb-CAPs toolbox (Bolton et al., 2020b). The data was pre-processed using custom MATLAB (MATLAB 2019b) scripts and SPM12 functions (Wellcome Department of Cognitive Neurology, Institute of Neurology, UCL, London, UK). Volumes were realigned to the first scan, and spatially smoothed with a gaussian filter (FWHM = 6 mm), after being normalized to MNI space. Then, linear trends were removed from each voxel's time course, and such time courses were further temporally z-scored.

The first step of CAPs analysis requires the selection of one or more seed regions in order to identify timepoints when these seeds exhibit high BOLD signal. As seeds we considered the right pSTS and right IFG, which are the only two regions that were previously reported to be more active in the asynchronous condition (where PH and PE are induced) than in the synchronous condition, and are part of a functionally impaired network in neurological patients experiencing symptomatic PH (Bernasconi et al., 2021). In the second step of the analysis, timepoints of any of the two seed regions where activity exceeded a z-score of 1, were marked and considered for further analysis. To deal with head motion, timepoints with a framewise displacement above 0.5 mm were scrubbed (Power et al., 2012). In the third step, the volumes (frames) of the selected timepoints were fed into a k-means algorithm to obtain temporal clusters based on spatial patterns. The best k was selected beforehand through consensus clustering which provides stability measures for data points being clustered together across different numbers of selected centroids (Monti et al., 2003). In the fourth and final step, all frames assigned to the same label were averaged to obtain a representative CAP. The frames of timepoints when none of the seeds were active are averaged in a non-active state, CAP_0. Finally, each timepoint is tagged, taking into account haemodynamic lag of 2 TRs, to one of the three experimental conditions: asynchronous sensorimotor manipulation, synchronous sensorimotor manipulation, or rest.

2.5. Occupancy and average duration of the CAPs

For each CAP (CAP_1 to CAP_9) and for the non-active state (CAP_0), two metrics were computed during the different experimental conditions: occupancy and average duration (Chen et al., 2015). Let $CAP_i[k]$ be the binary time course that indicates if CAP i, is active at any timepoint k element of the set $D_{S,C}$ which contains all active, non-active, and scrubbed, timepoints of a condition C, for a single participant S. Occupancy refers to the percentage of scans a CAP i occupies in a given condition:

$$Occ(i; D_{S,C}) = \frac{\sum_{k \in D_{S,C}} CAP_i[k]}{|D_{S,C}|}.$$

We define $CAPDur_i[r]$ as the duration (number of consecutive timepoints active) of CAP i for each associated occurrence r. Average duration is the mean CAP duration for each participant:

$$AvgDur(i; D_S) = \overline{CAPDur_i(r)}.$$

With the main goal of identifying specific CAP behaviour in the asynchronous versus synchronous condition, as well as its association with PH and PE, CAPs' occupancies were tested across conditions by means of a non-parametric ANOVA (Friedman's test). When significant effects were observed, this was followed by post-hoc non-parametric tests of the medians (i.e., Wilcoxon rank sum test) for each of the CAPs to reveal significant changes in occupancy with the experimental different conditions. These results were corrected for the false discovery rate (FDR) with the Benjamini-Hochberg procedure (Benjamini and Hochberg, 1995) to correct for multiple comparisons (i.e., number of CAPs).

The average duration of a CAP was only computed for the actual occurrences of a CAP. If a CAP never occurred for a participant in a specific condition, that measure of average duration was not considered zero, but rather the participant was excluded for the assessment of that specific measure. As consequence the number of measures of average duration, per CAP and per condition, was not always equal to the number

of participants. These different sample sizes meant that average duration could not be tested with a Friedman's test. We hence, tested average duration with Linear Mixed Models (LMM), using the *lmer* function provided with the package *lme4* (Bates et al., 2015) available for R (version 3.6.1). The average duration was modelled as a function of CAP, condition, interaction between CAP and condition, and a random-intercept accounting for inter-participant variability.

$$AvgDur \sim (1|Participant) + CAP + Condition + CAP : Condition$$

The parameters of the model were tested for significance by sequential comparison of the simplest model with only the random-participant intercept against a model adding the CAP parameter, followed by comparing the latter model with one adding the condition parameter, and finally comparing this one with the full model that includes the interaction parameter. Comparisons were performed with the Wald χ^2 test (Liu, 2016). If an interaction was detected, the effect of condition on average duration was then investigated for each CAP.

If a CAP was found to have higher occupancy or average duration in the asynchronous condition, Spearman's correlations were used to investigate potential relationships between that CAP's occupancy or average duration and the strength of the subjective experiences of PH and PE.

2.6. Transition probabilities between the CAPs

To characterize temporal relationships between CAPs, we computed transition probabilities (TPs) that describe the probability of a CAP to transition to itself, to another CAP, or to the non-active state (CAP_0). Per condition and per participant, the TPs of an initial CAP i to a next CAP j are computed by normalising the number of times a starting CAP i transitions to a next CAP j, by the number of times the initial CAP i occurs:

$$TP(i, j; D_S) = \frac{\sum_{k \in D_S} \mathrm{CAP}_i[k]\mathrm{CAP}_j[k+1]}{\sum_{k \in D_S} \mathrm{CAP}_i[k]}.$$

The TPs can then be organized per participant and condition into a 10×10 matrix, which will be considered as the TP matrix characterizing a first-order Markov chain modelling the sequence of CAPs.

The goal was now to investigate if the Markov model changes, under different experimental conditions, and between the subgroups of participants who are sensitive (or not) to PH and/or PE induction. To that aim, we modelled the TPs with LMM. Our approach to this problem can be described as a three-step hierarchical analysis of the factors that can influence TPs.

We first modelled the TPs based on the initial and next CAPs involved in each transition. This implied modelling the data with a fixed-effect parameter for the initial CAP, a fixed-effect parameter for the next CAP, and an interaction parameter for the initial and next CAPs. Between-participant variability is accounted for in the model with a random intercept:

$$TP \sim (1|Participant) + CAP_{init} + CAP_{next} + CAP_{init} : CAP_{next}$$

$$TP \sim (1|Participant) + CAP_{init} + CAP_{next} + CAP_{init}{:}\,CAP_{next}$$

I

II

III

We assessed how each parameter improved the explained variance of the data, by consecutive comparisons of increasingly complex models (0, I, II, III) with a Wald χ^2 test. Model 0 only comprised a random-effect parameter for between participant variability. Model I included in addition, a fixed-effect parameter for the initial CAP (i.e., row in the TP matrix). Model II added a fixed-effect parameter for the next CAP (i.e., column in the TP matrix). And Model III added the interaction between the initial and the next CAP, which expresses that TPs for each pair of CAPs can be different. For this group of models (and for all subsequent groups of models) we report the variation of Akaike Information Criteria (ΔAIC; Akaike, 1974), which gives an indication of goodness-of-fit penalised by the complexity of the model. For clarity this variation should be negative if a model higher variance explanation compensates its higher complexity (as compared to another less complex model, which also explains variance but to a lesser degree).

In case Model III revealed a significant effect of the interaction parameter, we continued with the second step of the analysis. We divided the subsequent analysis into two parts. First, fixing a specific initial CAP (i.e., row of the TP matrix) to investigate forward properties of the Markov models, and second, fixing a specific next CAP (i.e., column of the TP matrix) to investigate backward properties of the Markov models. For this analysis we limited the division in specific initial CAP, or specific next CAP, to CAPs that are more prominent during the sensorimotor task (i.e. significantly higher Occurrences and/or Average Duration, during the asynchronous and synchronous conditions rather than rest). However, the variables, $\mathrm{CAP}_{\mathrm{next}}$ in the forward properties model, and $\mathrm{CAP}_{\mathrm{init}}$ in the backward properties model, represented all possible states (inactive state and CAPs). The corresponding LMMs are represented as follows, with F or B representing the forward or backward properties, and i the fixed initial or next CAP:

Forward Properties $TP(CAP_{init} = CAP_i) \sim (1|Participant) + CAP_{next} + Cond + PH + Cond : PH$

Forward Properties $TP(CAP_{init} = CAP_i) \sim (1|Participant) + CAP_{next} + Cond + PH + Cond{:}\,PH$

F_i 0

F_i I

F_i II (PH)

F_i III (PH)

Backward Properties $TP(CAP_{next} = CAP_i) \sim (1|Participant) + CAP_{init} + Cond + PH + Cond : PH$

Backward Properties $TP(CAP_{next} = CAP_i) \sim (1|Participant) + CAP_{init} + Cond + PH + Cond{:}\,PH$

B_i 0

B_i I

B_i II (PH)

B_i III (PH)

These models included the effects of, condition, sensitivity to PH induction (positive PH-strength score), and interaction between these two. The sensitivity to the induction of the PH can be interpreted as a group variable as it is a binary value. To assess the effect of sensitivity to PE induction (positive PE-strength score) and interaction with condition, another set of models was used (for F_i and B_i, Models II and III). This was due to convergence not being achieved with the current amount of data available if both PH, PE, and respective interactions with conditions, are analysed simultaneously. To compensate for this, we lowered the significance threshold of the subsequent Wald χ^2 tests to 0.025, instead of 0.05. As before, the effect of each model's parameters was assessed by sequentially comparing simpler models and more complex models, e.g. from Model B_i 0 to Model B_i III (PH), using the Wald χ^2 test. These results were corrected for FDR with the Benjamini-Hochberg procedure to correct for multiple comparisons (i.e., number of assessed transitions by number of induced illusions).

Finally, if a significant effect of the interaction between condition and sensitivity to PH-induction or to PE-induction, was observed for a specific B_i III Model, then that model continued into the third and last step of the analysis. Here, to properly investigate the effect of sensitivity to PH or PE induction on the TPs over different conditions, the models also fixed the conditions (these models will have C added in the notation, as in F_i^c(PE) with C taking the values *a, s* or *r,* identifying the asynchronous, synchronous or rest condition, respectively). Results were corrected for multiple comparisons using the Benjamini-Hochberg procedure, simultaneously for the number of conditions times the number of independent models. An example for investigating the effect of

sensitivity to PH-induction, on the TPs of a specific $CAP_{next} = CAP_i$ in the synchronous condition, is the following model:

$$TP\left(CAP_{next} = CAP_i,\ Cond = \ Sync\right) \sim (1|Participant) + CAP_{next} + PH.$$

2.7. Control analyses

In order to account for potential confounds in our analysis and test the specificity temporal metrics of the CAPs associated with the pSTS and IFG, we ran two additional CAP analyses. Both analyses follow the analysis protocol described in the previous sub-chapters, however, the CAPs clustering procedure is based on control regions instead of our regions of interest: pSTS and IFG.

The first control analysis is intended to control for known intrinsic brain networks. For this analysis we performed CAPs clustering based on the activity of the posterior cingulate cortex (PCC), an area known to recover sub-states of a major intrinsic brain network, the default-mode network (DMN; Shirer et al., 2012).

The second control analysis is intended to control for other regions that are known to be associated with the asynchronous condition (i.e. more active in this condition compared to the synchronous condition), but potentially not associated with PH. Besides the pSTS and IFG, both the anterior insula (aINS) and the medial superior frontal gyrus (mSFG), showed higher activity in the asynchronous condition when compared to the synchronous one (Bernasconi et al., 2021). However, in contrast to the pSTS and IFG, these two regions (aINS and mSFG), did not overlap with the functionally impaired network extracted from neurological patients afflicted with PH (Bernasconi et al., 2021). Consequently, we hypothesize that CAPs associated with these regions might show a task modulation, but should not be related to PH/PE.

3. Results

3.1. CAP analysis reveals multiple distinct spatial patterns

With CAP analysis, we explored how different CAPs occurred and interacted under different experimental conditions, and, secondly, how this was associated with the level of the subjective experience of PH and PE. The identified CAPs consisted of brain regions co-activating with one or both seeds, during periods in which at least one of the seeds was active (z-score above 1). The IFG seed was considered active on average 14.7% (SD: ± 2.9) of the total timepoints of the entire experiment (i.e., all sequential periods of rest, robot manipulation in the asynchronous condition, robot manipulation in the synchronous condition; in their original order for each participant, respectively). A similar percentage of 15.0% (SD: ± 2.1) was found to be active for the pSTS seed. On average, 23.6% (SD: ± 3.4) of all timepoints were selected, given that seed activity overlapped at given times. The remaining timepoints were assigned to the non-active state, with only 0.4% (SD: ± 1.0%) being scrubbed. Following timepoint selection, consensus clustering was run to determine the best number of centroids for the clustering procedure. The stability measure assessed with this method recommended segregating the data into 9 centroids (Supplementary Fig. S1). Hence, CAPs analysis was applied to the selected timepoints revealing nine different co-activation patterns (Supplementary Fig. S2 and Table S2, for description of cluster peaks), for which occupancy, average duration, and TPs were explored (see below).

3.2. Sensorimotor conditions alter CAPs occupancy and average duration

Here, we will first focus on the analysis of a CAP's occupancy (percentage of a CAP occurrence in a condition) and a CAP's average duration (number of seconds a CAP lasts on average, once it occurs) across the two sensorimotor conditions and rest.

Occupancy. Friedman's test revealed a significant difference in occupancy of CAPs between the conditions of asynchrony, synchrony, and rest (p-value = 0.020). Follow-up multiple comparison corrected post-hoc tests revealed that several CAPs changed their occupancy depending on the condition (Fig. 2A). CAP 6 was the only CAP to show a higher occupancy in the asynchronous condition, when compared to both the synchronous condition (p-value = 0.049) and to rest (p-value = 0.002). This CAP's increase in occupancy between the asynchronous and synchronous condition did not show any significant correlation with the strength of the subjective experiences of PH ($\rho = 0.10$, p-value = 0.630) or with PE ($\rho = 0.23$, p-value = 0.280). CAP 7 and CAP 9 had a significantly higher occupancy for both asynchronous and synchronous conditions, when compared to rest (both p-values < 0.001). However, the occupancy of these two CAPs did not differ between the asynchronous and synchronous conditions. A summary of the occupancy results for all remaining CAPs can be seen in the Supplementary Table S3.

Average duration. Linear mixed models fixed-effect statistics revealed a significant effect of CAP on the average duration (p-value < 0.001), showing that different CAPs have different average durations. A significant effect of condition was also identified (p-value < 0.001), indicating that the experimental conditions significantly changed the average durations of the CAPs. Crucially, a significant interaction between CAP and condition was observed (p-value < 0.001), showing that the experimental conditions affected the average duration of each CAP differently. To further investigate this interaction, we ran post-hoc tests for the effect of condition on each CAP (Fig. 2B). CAP 6 showed a significant difference in average duration across the conditions, with the asynchronous condition having a higher average duration than the synchronous condition and rest (estimate in asynchronous condition: 3.56, SE = ±0.17, t-value = 20.66; estimate effect of synchronous condition: −0.60, SE = ±0.24, t-value = −2.55; estimate effect of rest: - 0.57, SE = ±0.24, t-value = −2.33; p-value = 0.021). This increase of average duration did not show any correlation with the strength of the induced PH ($\rho = 0.06$, p-value = 0.78), nor that of PE ($\rho = 0.05$, p-value = 0.78). CAP 7 also showed a significant difference in average duration across the conditions, with the asynchronous condition having a higher average duration than the synchronous condition and rest, and the synchronous condition also lasting longer than rest (estimate in asynchronous condition: 3.41, SE = ±0.16; t-value = 21.81 estimate effect of synchronous condition: −0.30, SE = ±0.22, t-value = −1.40; estimate effect of rest: - 0.64, SE = ±0.22, t-value = −2.95; p-value = 0.015). This increase of average duration for CAP 7 did not show any correlations with the strength of induced PH ($\rho = 0.04$, p-value = 0.84), nor that of induced PE ($\rho = 0.12$, p-value = 0.55). The values for all other CAPs were not characterized by significant results (p-value > 0.05) and are summarised in Supplementary Table S4.

Brain activation for Co-Activation Pattern 6. The network identified as CAP 6 (Fig. 3A) is composed by ten brain regions, with its main components in the right pSTS, bilateral inferior parietal lobule (IPL, centred on the angular gyrus, AG), the right dorso-lateral prefrontal cortex (dlPFC), which included the IFG region used as seed, and the middle prefrontal cortex (mPFC; including part of the supplemental motor area, SMA). Smaller cortical regions were found in the left dlPFC and left premotor cortex. Subcortical activations were detected in the right caudate and the cerebellum (left Crus I and II). Deactivations were observed in the cuneus and the occipital gyrus.

3.3. Experience of PH changes CAPs' transition probabilities

Next, we investigated to what extent CAPs' transitions are affected by the experimental conditions (asynchronous, synchronous, rest) and by sensitivity to the induction of PH and PE (more information on the model's results in supplementary table S5).

In the first step of this analysis, we assessed whether TPs depended on the initial and next CAP, by comparing the first three models. Linear mixed models fixed-effect statistics revealed significant effects for all the parameters associated with transitions between CAPs. Specifically, Model I revealed a significant effect of the initial CAP (p-val = 0.009,

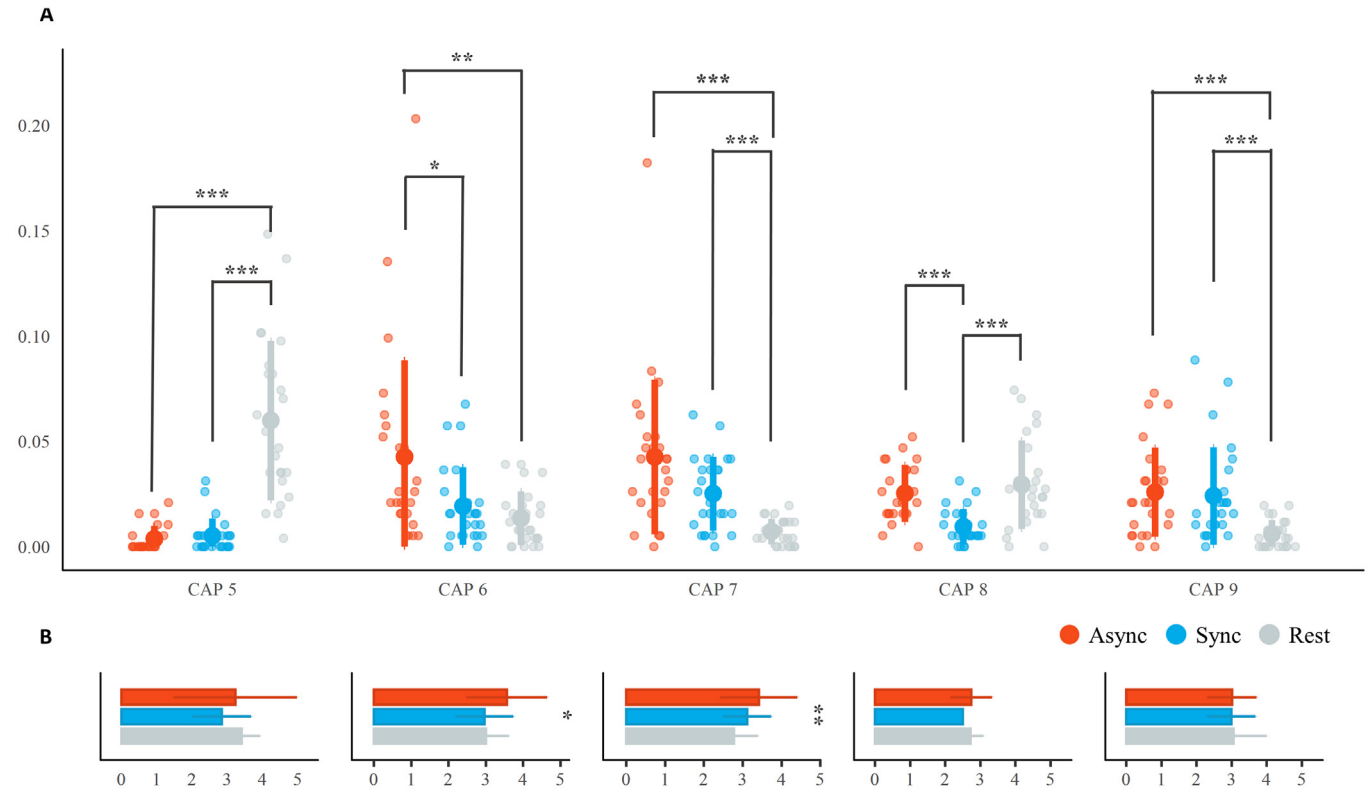

Fig. 2. Occupancy and average duration of the CAPs
(A) The occupancy of CAPs 5 to 9 in the different conditions. While CAPs 7 and 9 were associated with the sensorimotor conditions, CAP 6 showed a significantly higher occupancy for the asynchronous condition as compared to synchrony (and rest), denoting its specificity to the temporal conflict present in the asynchronous condition. **(B)** The average duration of CAPs 5 to 9. Only CAPs 6 and 7 show an effect of condition on the average duration, with CAP 6 lasting more in the asynchronous condition, and CAP 7 lasting more, the more sensorimotor conflicts are introduced. (*p-value < 0.05; **p-value < 0.01; ***p-value < 0.001).

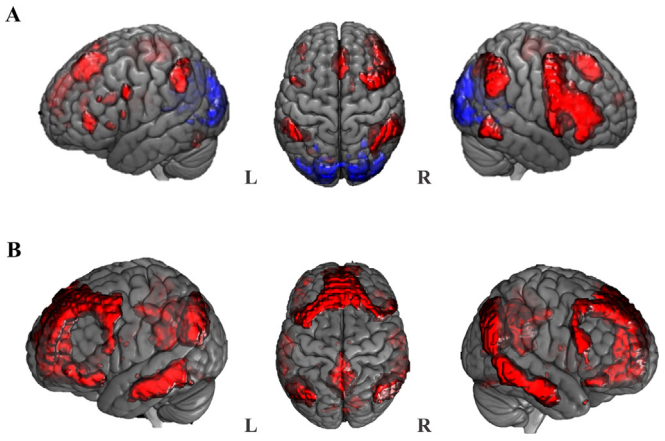

Fig. 3. Anatomy of CAP 6 (PH) and CAP 9 (PE)
(A) Brain regions of CAP 6 are shown involving the right posterior superior temporal sulcus, the bilateral inferior parietal lobule with focus on the angular gyri, the right dorso-lateral prefrontal cortex, the middle prefrontal cortex (including part of the supplemental motor area), the left dorso-lateral prefrontal cortex, the left precentral gyrus, the body of the caudate on the right, and in the cerebellum, the left Crus I and II. Deactivations are observed over the cuneus and occipital gyrus. **(B)** Brain regions of CAP 9 are shown in posterior cingulate cortex, middle prefrontal cortex and bilateral posterior parietal cortex. This CAP extends from the DMN with clusters over the superior and middle frontal gyrus, bilateral clusters on the middle temporal gyrus, and bilateral clusters on the Crus I and II of the cerebellum. Two small clusters are also observed in the thalamus.

ΔAIC = −3.7), showing that CAPs' TPs will change depending on the initial CAP of the transition. Model II revealed a significant effect of the next CAP (p-val < 0.001, ΔAIC = −4660.4), showing that CAPs' TPs also depended on which CAP they are transitioning to. Finally, Model III revealed a significant interaction effect between the initial CAP and next CAP of a transition (p-val < 0.001, ΔAIC = −865.5), showing that TPs are dependant on the specific combination of initial and next CAP. Given this interaction effect, we proceeded with the analysis of the remaining parameters of condition, PH sensitivity, and PE sensitivity, and did so separately for each value of initial (forward properties) and next (backward properties) CAP.

Forward properties. Here we focused on analysing the remaining parameters mentioned above, for each fixed initial CAP level ($CAP_{init} = CAP_i$). By doing so, Models F_i I revealed a significant effect of condition (Fig. 4A, B, C, Supplementary Fig. S3) for transitions beginning in CAP_{init} 9 (p-value = 0.008, ΔAIC = −7.8), as seen in Fig. 4D. The remaining models, F_i II (PH) and F_i III (PH), showed that PH sensitivity did not significantly change the TPs, nor did its interaction with condition. Sensitivity to PE also did not show any significant effect (F_i II (PE)), nor did the interaction of this parameter with condition (F_i III (PE)). Overall, the experimental conditions, have a small effect on how the TPs change when departing from initial CAP 9, however no effect was observed for sensitivity to PH or to PE.

Backward properties. Here we focused on analysing the same parameters mentioned above, but for each fixed next CAP level ($CAP_{next} = CAP_i$). Models B_i I revealed a main effect of condition (Fig. 4A, B, C, Supplementary Fig. S3) for transitions ending in CAP_{next} 6 (p-value < 0.001, ΔAIC = −16.89), CAP_{next} 7 (p-value < 0.001, ΔAIC = −11.7), and CAP_{next} 9 (p-value = 0.006, ΔAIC = −6.2), as seen in Fig. 4E. PH sensitivity did not have a significant effect for any of the B_i II (PH) Models. However, Models B_i III (PH) detected a significant interaction effect

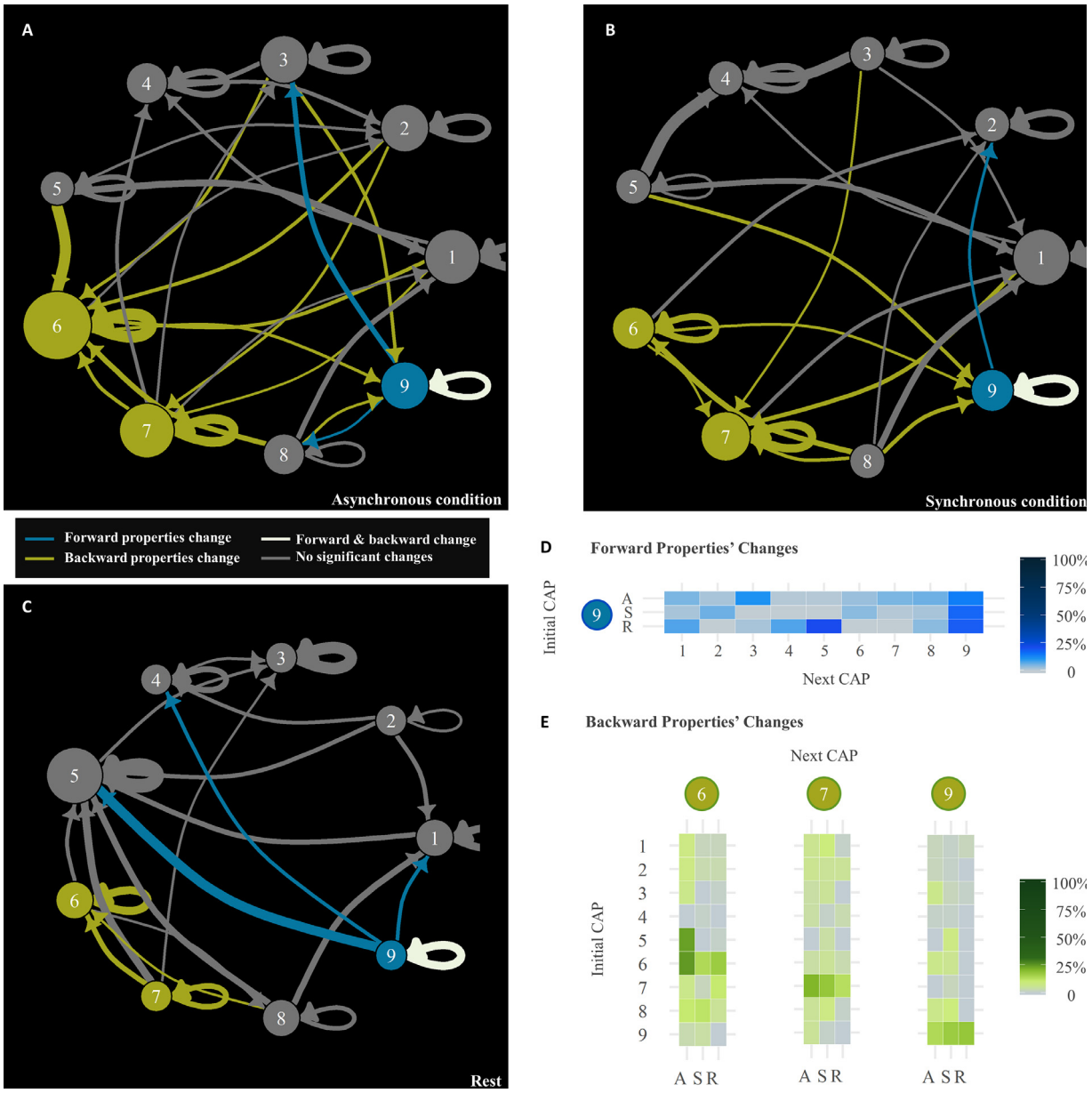

Fig. 4. CAPs' Transition Dynamics across different conditions
Transitions that occur at least 5% of the time for each CAP, are shown across the different conditions. Highlighted in blue are CAPs that changed forward properties significantly across conditions. Transitions departing from such CAPs are also depicted in blue. Highlighted in green are CAPs that changed their backward properties significantly across conditions. Transitions arriving at such CAPs are also depicted in blue. Coloured in white, are the transitions departing from an initial CAP with significant changes in forward properties, and arriving at a next CAP with significant changes in backward properties. CAPs in grey did not change properties across conditions. The size of each CAP is proportional to the amount of arriving and departing transitions. The size of each transition is related to its probability. **(A)** Asynchronous condition. **(B)** Synchronous condition. **(C)** Rest. **(D)** changes in forward properties' across conditions (A - Asynchronous; S - Synchronous; R - Rest), can be seen in detail from CAP 9 to all the other CAPs. **(E)** Changes in backward properties' across condition, can be seen in detail for transitions from every CAP, to CAPs 6, 7, and 9.

between condition and PH sensitivity, for the transitions to CAP_{next} 6 (p-value = 0.036, ΔAIC = −4.85). Regarding PE, no main effect was found, but, crucially, a significant interaction between PE and condition was observed for the transitions to CAP_{next} 9 (B_i III (PE); p-value = 0.026, ΔAIC = −5.5). Overall, the experimental conditions, have a widespread effect on how the overall TPs of every CAP, when transitioning to CAPs 6, 7, and 9. Moreover, CAP 6 was linked to PH and CAP 9 to PE.

Observing an interaction between PH sensitivity and condition implied that the effect of being sensitive to PH induction varied with the experimental condition, but only for TPs ending in CAP 6. Hence, to better investigate the effect of PH sensitivity, we analysed each condition independently, for the transitions ending in CAP 6. Models B_i^c I (PH) revealed a significant effect PH sensitivity in the asynchronous condition for transitions ending in CAP_{next} 6 (estimate = 0.072, SE = ± 0.029, p-value = 0.039, ΔAIC = −4.12, Fig. 5A, Supplementary Fig. S4), but not in the synchronous condition (estimate = 0.008, SE = ±0.016, p-value = 0.59, ΔAIC = +1.71, Fig. 5B, Supplementary Fig. S4), nor in rest (estimate = 0.012, SE = ±0.018, p-value = 0.47, ΔAIC = +1.48). This showed that during PH induction, most CAPs will have an increase in the transition probability to CAP 6 (Fig. 3A). Consequently, and observed only in the asynchronous condition, the PH induction puts the brain's transition probabilities between different brain patterns, in a temporary

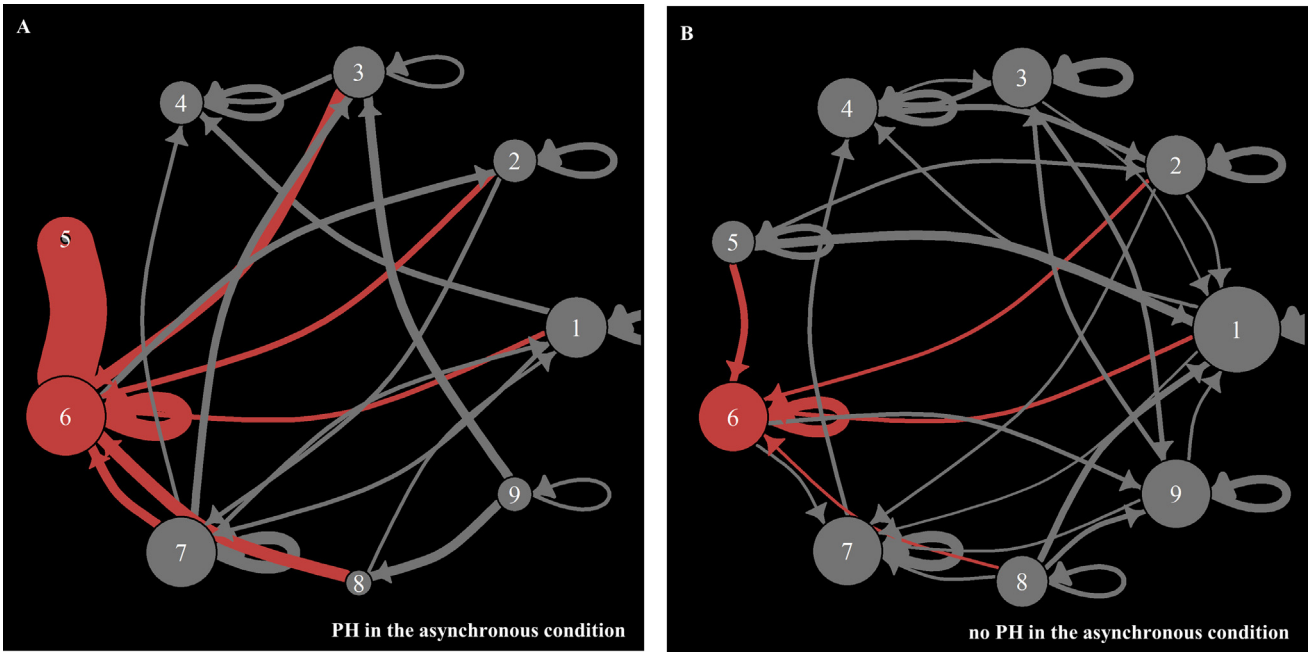

Fig. 5. PH transition dynamics
Transitions that occur at least 5% of the time for each CAP, are shown in the asynchronous condition for different sensitivities to the induction of PH. Highlighted in red are CAPs that significantly changed backward properties depending on the sensitivity to PH. Transitions arriving at such CAPs are also depicted in red. **(A)** CAPs' transitions in the asynchronous condition when a PH is experienced **(B)** CAPs' transitions in the asynchronous condition without PH. The induction of a PH significantly increases the transition probabilities of the CAPs to CAP 6, resulting in a high convergence of the other CAPs to CAP 6, which is not seen if a PH is not experienced.

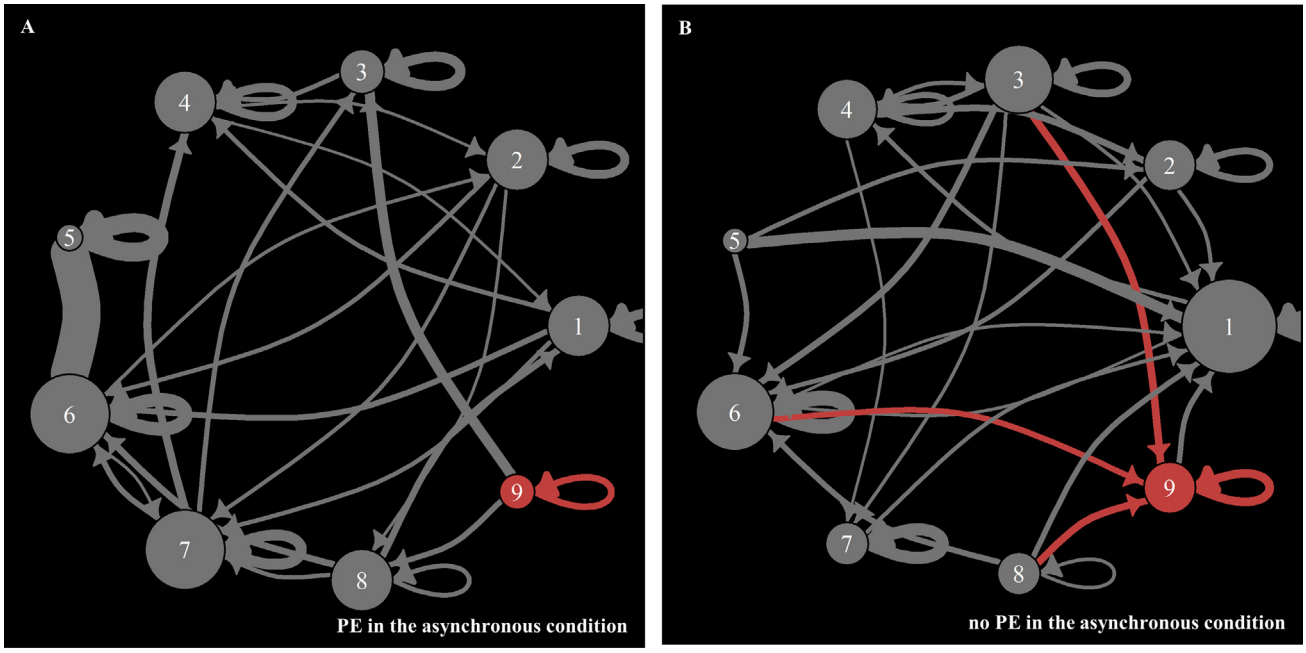

Fig. 6. PE transition dynamics
Transitions that occur at least 5% of the time for each CAP, are shown in the asynchronous condition for different sensitivities to the induction of PE. Highlighted in red are CAPs that significantly changed backward properties depending on the sensitivity to PE. **(A)** CAPs' transitions in the asynchronous condition when a PE is experienced **(B)** CAPs' transitions in the asynchronous condition without PE. Transitions arriving at such CAPs are also depicted in red. The induction of PE significantly decreases the transition probabilities of the CAPs to CAP 9.

dynamic arrangement, in which CAPs predominantly transition to CAP 6.

Observing an interaction between PE sensitivity and condition implied that the effect of being sensitive to PE induction varied with the experimental condition, only for the TPs ending in CAP 9. In the same way as for PH, we analysed the PE factor independently for each condition, for the transitions ending in CAP 9. Models $B_9{}^c$ I (PE) revealed a significant effect of PE sensitivity on the transitions to CAP_{next} 9 in the asynchronous condition (estimate = −0.05, SE = ±0.02, p-value = 0.030, ΔAIC = −4.62, Fig. 6A, Supplementary Fig. S5), but not in the synchronous condition (estimate = 0.005, SE = ±0.017, p-value = 0.76, ΔAIC = +1.21, Fig. 6B, Supplementary Fig. S5) nor in rest

(estimate = 0.002, SE = ± 0.008, p-value = 0.77, ΔAIC = + 1.91). This showed that if a participant is sensitive to PE induction, most CAPs will decrease their probability of transitioning to CAP 9, in the asynchronous condition.

Brain activation for Co-Activation Pattern 9. The network identified as CAP 9 (Fig. 3B), contains significant clusters over the mPFC, precuneus, posterior cingulate cortex (PCC), bilateral AG, bilateral superior and middle frontal gyrus, as well as two bilateral clusters in the STS region. Subcortical clusters included bilateral thalamus and the bilateral cerebellum (Crus I and II).

3.4. Control analyses

Posterior Cingulate Cortex. The CAPs clustering procedure for this analysis was done for only 6 centroids, as this was the recommended value by its own consensus clustering metrics (Supplementary Fig. S6). From the analysis of the occupancies and average durations of the obtained CAPs, no single CAP showed specificity to the sensorimotor conditions (all CAP p-values > 0.05). All details on the statistical analysis for this control analysis can be found in the supplementary material (Supplementary Table S6).

Anterior Insula and Medial Superior Frontal Gyrus. The CAPs clustering procedure for this analysis was also done for 9 centroids, as recommended by its own consensus clustering metrics (Supplementary Fig. S7). From the analysis of the occupancies and average durations of the obtained CAPs, only one such CAP showed to be specific to the sensorimotor conditions (in this case CAP aINS-mSFG-2, showed a significant increase in average duration during the conditions, p-value < 0.05, ΔAIC = −9.62). When analysed for TPs, this CAP did not show any interaction between condition, and PH or PE (Forward properties – condition and PH: p-value = 0.74; Forward properties – condition and PE: p-value = 0.78; Backward properties – condition and PH: p-value = 0.50; Backward properties – condition and PE: p-value = 0.19). All details on the statistical analysis for this control analysis can be found in the supplementary material (Supplementary Tables S7 and S8).

4. Discussion

In the present work we applied recent advances in dynamic functional connectivity methods, to fMRI of brain activity, to explore fluctuating brain states during a novel paradigm linking MR-compatible robotics and fMRI, used to control the subjective mental states of PH and PE in healthy individuals. We were able to identify two brain patterns, CAP 6 and CAP 9, which were both induced by the sensorimotor tasks, and sensitive to PH or PE, respectively. Such sensitivity was revealed as a temporal rearrangement of brain activity by altered transition probabilities that favoured CAP 6 in the event of PH and avoided CAP 9 in the event of PE. These data demonstrate that changes in transition dynamics of a specific network underlie the experience of a PH, and that such changes are independent of the experience of PE which in many participants accompanies PH.

4.1. Neural correlates of the PH-induction

A previous study has identified brain regions that in healthy participants are more active in the asynchronous condition (where PH and PE occur) rather than in the synchronous one, and further linked them with the PH through lesion network mapping analysis in neurological patients reporting PH (Bernasconi et al., 2021). Here, we identify a brain pattern, CAP 6, that has significantly higher occupancy and average duration in the asynchronous condition. We argue that this reveals the sensitivity of CAP 6 to the temporal delay present in the asynchronous condition, whereas other CAPs, such as 7 and 9, are modulated by the sensorimotor stimulation per se, and independently of the delay, given their higher occupancies and longer average durations for both asynchronous and synchronous conditions as compared to rest. These results show that asynchronous sensorimotor stimulation modulates a brain network that includes brain regions previously associated to PH (Bernasconi et al., 2021).

The findings presented here, specifically the analysis of the CAPs transition probabilities, further demonstrate that the induction of PH in the asynchronous condition is related to a significant change in how CAPs transition amongst themselves. Only during the asynchronous condition and only in the participants who are sensitive to PH-induction (i.e. higher PH ratings in the asynchronous versus synchronous condition) do we observe a significant increase in transition probabilities from all CAPs to CAP 6, as if this CAP is neurally “attracting” the other CAPs (Fig. 5A). Accordingly, we argue that PH induction can be characterized by a perturbation of the “normal” brain network dynamics, consisting in an increase of the probability of all CAPs transitioning to CAP 6. No such changes in transition probabilities are observed in the synchronous condition, rest, nor in the control analyses performed with both control groups of control seed regions. Moreover, the fact that this CAP 6 change is not associated with the closely related conscious experience of PE, provides a disambiguation of the neural underpinnings of PH from those of PE (which are discussed in a subsequent section), even if PH is behaviourally, as tested by the present robotic system, typically accompanied by PE.

CAP 6 mainly consists of the right pSTS, the right dlPFC (including the IFG seed), the mPFC (including the SMA), and the bilateral AG. The former two areas (used as seeds in this analysis) have been previously linked to the PH (Arzy et al., 2006a; Blanke et al., 2014; Bernasconi et al., 2021). In addition, the pSTS is a multisensory and sensorimotor brain region which responds to tactile, visual and auditory stimuli (Beauchamp et al., 2008), as well as movement-related processes (Zito et al., 2020) and multisensory hallucinations (Ghazanfar and Schroeder, 2006). The mPFC cluster in CAP 6 has often been associated with different self-related processes (Gusnard et al., 2001; Platek et al., 2006; Beer et al., 2010; Whitfield-Gabrieli et al., 2011). In particular, a meta-analysis investigating the role of self-related, familiar, and other-related stimuli, identified this mPFC cluster as the main brain region distinguishing between self and other related processing (Qin and Northoff, 2011). We further note that the mPFC cluster includes the SMA, a region which has been implicated in bodily self-consciousness (i.e. Ferri et al., 2012; Ionta et al., 2013). The involvement of the bilateral AG has also been previously linked to PH, given that lesions in this area are associated with PH (Blanke et al., 2014). Finally, the deactivations we observe in the present study over the cuneus and occipital gyrus, which represent decreased BOLD in the secondary visual network (Shirer et al., 2012), are likely to be associated with opposing fluctuations between different functional networks (Fox and Raichle, 2007).

Disturbed interactions between functional networks have been hypothesized to represent a neural mechanism associated with several psychotic processes (Menon, 2011). Previous work suggested that hallucinations occur due to erroneous switches between two intrinsic networks, the central executive network (CEN) and default-mode network (DMN) (Menon and Uddin, 2010; Goulden et al., 2014). In particular, recent research showed that, when comparing hallucination and no-hallucination periods in schizophrenia, the interactions between major intrinsic networks follow different transition rules (Lefebvre et al., 2016). Similar mechanisms have also been proposed for Parkinson patients suffering from psychosis (Shine et al., 2014, 2015; Ffytche et al., 2017), a population typically afflicted by PH (Fénelon et al., 2011). The present data are compatible with that proposal. However, while previous work compared patients with hallucinations versus patients without hallucinations or patients with versus without psychosis, we report data in healthy participants in whom a specific hallucination, PH, is induced experimentally and in controlled fashion. Our data demonstrates, under the form of altered transition probabilities, that the induction of PH leads to aberrantly increased transitions to CAP 6, and that, by consequence, significantly different network interactions are observed between participants sensitive and those insensitive to PH induction. These results pro-

vide further evidence that hallucinations result from erroneous network switches (Goulden et al., 2014; Lefebvre et al., 2016) and extend this proposal to experimentally controlled hallucinations in healthy individuals.

4.2. Neural correlates of the PE-induction

Most participants that were sensitivity to the induction of PH during the asynchronous condition of the sensorimotor task, experienced it with the accompanying sensation of PE. However, several participants that did not experience robot-induced PH in the asynchronous condition, nevertheless reported PE. Despite the strong link between these two sensations when being robotically induced in healthy individuals, the occurrence of PE without PH, paired with the use of dFC methods, allowed us to identify the different neural mechanisms that underlie both experiences. Although we observe three CAPs that have their occupancy and average duration modulated by the sensorimotor task (CAP 6, CAP 7, CAP 9), we find that only the change in the transition probabilities to CAP 9 is associated with PE. Distinctly from the induction of the PH, where all CAPs increase their transition probabilities to CAP 6, the induction of PE in the asynchronous condition is characterised by a significant decrease of the transition probabilities of all CAPs to CAP 9, suggesting that this brain pattern is generally avoided in the event of PE. No such significant changes in transition probabilities to CAP 9 are observed in the synchronous condition, rest, nor in the control analyses performed with both groups of control seed regions.

CAP 9 overlaps in three main regions with CAP 6; i.e., the pSTS, mPFC, and bilateral AG. Besides the implications that have been proposed for the latter component in PH, we consider a possible dual role of this region, given that the AG has been extensively implicated in PE both in healthy individuals (Farrer and Frith, 2002; Blakemore et al., 2003), and in patients with schizophrenia and symptomatic passivity experiences (Farrer et al., 2004). In addition to these common regions, CAP 9 also includes the precuneus, the PCC, extensions of the pSTS activation over the middle temporal gyrus, and the mPFC cluster, which here does not include the SMA and is significantly larger than in CAP 6, extending to midline cortical structures over the ventral and dorsal medial prefrontal cortexes. The presence of the bilateral AG, precuneus, PPC, together with the observed midline cortical structures, which overlap significantly with the midline cortical structures of the DMN (Raichle et al., 2001; Shirer et al., 2012), suggest that the brain pattern of CAP 9 is closely related to the DMN. This is consistent with previous studies using the same or similar dFC methods, which recovered either parts or the complete DMN (Kiviniemi et al., 2011; Liu and Duyn, 2013; Liu et al., 2018). Diminished network interactions with the DMN in hallucinations have been reported before; e.g., in first-episode psychosis patients (Jardri et al., 2013), and in schizophrenic patients with positive symptoms (Lefebvre et al., 2016), both spontaneously hallucinating during resting state fMRI. The effect observed here for PE, with most CAPs decreasing their transition probabilities to CAP 9, contrasts with our initial prediction that PE, as PH, would be grounded on a dominance of a brain state over another. However, shunning of specific networks is known in hallucinations, particularly for the DMN, as observed in psychotic patients (Jardri et al., 2013; Lefebvre et al., 2016). Due to the very significant number of features shared between the identified CAP 9 for which this mechanism occurs associated with PE, and the DMN, we do not exclude the possibility that what is detected here for PE-induction might be in fact a more general mechanism underlying hallucinations, beyond PE.

4.3. Mechanisms of PH and PE in robotically mediated induction of hallucinations

In the present work, we find that both the induction of PH and PE are characterized by significant changes in network interactions. We previously described two regions, pSTS and IFG, that were more active during robot-induced PH in the asynchronous condition (Bernasconi et al., 2021) and that also overlapped with an impaired functional network as defined in neurological patients with clinically-relevant PH. Based on the present findings, we propose that the activations of the pSTS and IFG in the asynchronous condition represent a general predisposition to the variations in network behaviour observed for CAP 6 and CAP 9, which lead to PH and PE respectively. Hence, in the asynchronous condition, the predisposition to having PH or PE is marked by such activations of the pSTS and IFG, but, importantly, PH and PE will only occur once the changes in network behaviour also occur. This view is supported by observations that certain brain regions can have a prominent role in the switching between different networks (Sridharan et al., 2008; Manoliu et al., 2014). In addition, hallucination processes in psychopathology also lend support to this hypothesis. Positive symptoms in schizophrenia and schizotypal disorders, can be marked by constant dysfunctions in functional connectivity between brain regions, that correlate with hallucination severity (Fletcher and Frith, 2009; Skudlarski et al., 2010; Ettinger et al., 2015), however, the occurrence of hallucinations is limited to time periods characterized by changes in network interactions (Lefebvre et al., 2016).

4.4. Methodological considerations

The study of dynamics of brain activity as measured by fMRI has received considerable attention during the past decade (Hutchison et al., 2013; Preti et al., 2017) and is particularly relevant to explain complex behaviour and psychopathology (Bolton et al., 2020a). In this work, we opted for CAPs analysis, which starts from the selection of relevant seeds, to probe their interaction with the rest of the brain in terms of dynamically occurring co-activation patterns. The most interesting alterations found in this study were characterized by transition probabilities, a rather subtle correlate of brain activity that has not yet been exploited to a big extent. More work is thus needed on this topic. There are also a number of limitations. First, we focused our analysis by choosing as seeds, two key brain regions previously identified for PH. While this approach allowed us to narrow down the scope of the measures, it might also be that other processes in the brain were missed. Second, the recovery of temporal dynamics by dFC methods, such as transitions between CAPs, might have been limited by the TR of 2.5 s that was chosen in the original study (Bernasconi et al., 2021). However, it is the haemodynamic response function that intrinsically limits the temporal dynamics (e.g., average durations are longer than 3 s), and, therefore, conventional TRs of 2–3 s are still useful to probe temporal processes between brain regions (Sahib et al., 2018). Third, temporal sequence analysis could be extended by generative models (Bolton et al., 2018; Vidaurre et al., 2017; Zhang et al., 2020), which can even be applied to individual nodes instead of at the network level (Bolton et al., 2020c). Another option would be to apply effective connectivity models, such as dynamic causal modelling (Friston, 2011) or Granger causality (Valdés-Sosa et al., 2005), which are used to infer inter-regional interactions supported by anatomical connections. Finally, future fMRI studies should determine the intensity of robot-induced PH and PE after each condition and across a larger range of sensorimotor stimulation conditions (i.e. as done in a behavioural task with patients in: Bernasconi et al., 2021) in order to measure and analyse the induced hallucinatory state in a more fine-grained manner.

5. Conclusion

In sum, we identify dynamic fluctuations of brain activity that underlie PH and PE in healthy participants. We show that, the robot-induced sensations in the asynchronous condition are characterized by subtle changes in brain pattern transitions. Whereas the asynchronous condition is characterized by increased activations of the pSTS and IFG, as well as higher occupancy and average duration of the network CAP 6,

for PH, we identify a significant increase of the probabilities for all observed brain patterns to transition to CAP 6, and for PE, we observe an avoidance of all observed brain patterns to transition to a partly overlapping, but different network, CAP 9. These results highlight the subtle neural changes of a specific network during robot-induced PH in healthy individuals and further disambiguate the brain processes of PH from those of the typically accompanying PE. Furthermore, we extend changes in network behaviour associated with clinically relevant hallucinations (Menon, 2011; Jardri et al., 2013; Lefebvre et al., 2016) to network behaviour during an experimentally-controlled specific hallucination, PH.

Data Statement

The research data used in this study was originally acquired in Bernasconi and Blondiaux, and colleagues (2021) Robot-induced hallucinations in Parkinson's disease depend on altered sensorimotor processing in fronto-temporal network. It can be found accessible through the link: https://zenodo.sorg/deposit/4423384

Declaration of Competing Interest

None.

Credit authorship contribution statement

Herberto Dhanis: Conceptualization, Methodology, Software, Formal analysis, Data curation, Writing – original draft, Writing – review & editing, Visualization. **Eva Blondiaux:** Supervision. **Thomas Bolton:** Methodology, Supervision. **Nathan Faivre:** Supervision. **Giulio Rognini:** Methodology. **Dimitri Van De Ville:** Conceptualization, Supervision, Writing – review & editing. **Olaf Blanke:** Conceptualization, Supervision, Writing – review & editing.

Acknowledgments

This work presented here was supported in by the Bertarelli Foundation, the Swiss National Science Foundation, the National Center of Competence in Research (NCCR) "Synapsy The Synaptic Bases of Mental Diseases" grant number 51NF40-185897, as well as by two generous donors advised by Carigest SA. The first of such donors wishes to remain anonymous, whilst the second one is the Fondazione Teofilo Rossi di Montelera e di Premuda.

Supplementary materials

Supplementary material associated with this article can be found, in the online version, at doi:10.1016/j.neuroimage.2021.118862.

References

Akaike, H., 1974. A new look at the statistical model identification. IEEE Trans. Automat. Contr. 19, 716–723. doi:10.1109/TAC.1974.1100705.

Arzy, S., Seeck, M., Ortigue, S., Spinelli, L., Blanke, O., 2006a. Induction of an illusory shadow person. Nature 443, 287. doi:10.1038/443287a.

Arzy, S., Thut, G., Mohr, C., Michel, C.M., Blanke, O., 2006b. Neural basis of embodiment: distinct contributions of temporoparietal junction and extrastriate body area. J. Neurosci. 26, 8074–8081. doi:10.1523/JNEUROSCI.0745-06.2006.

Bates, D., Mächler, M., Bolker, B.M., Walker, S.C., 2015. Fitting linear mixed-effects models using lme4. J. Stat. Softw. 67. doi:10.18637/jss.v067.i01.

Beauchamp, M.S., Yasar, N.E., Frye, R.E., Ro, T., 2008. Touch, sound and vision in human superior temporal sulcus. Neuroimage 41, 1011–1020. doi:10.1016/j.neuroimage.2008.03.015.

Beer, J.S., Lombardo, M.V., Bhanji, J.P., 2010. Roles of medial prefrontal cortex and orbitofrontal cortex in self-evaluation. J. Cogn. Neurosci. 22, 2108–2119. doi:10.1162/jocn.2009.21359.

Bejr-kasem, H., Pagonabarraga, J., Martínez-horta, S., Pérez-pérez, J., Angeles, M., Pascual-sedano, B., Gómez-ansón, B., Kulisevsky, J., 2018. Disruption of the default mode network and its intrinsic functional connectivity underlies minor hallucinations in Parkinson ' s disease 1–10. 10.1002/mds.27557

Benjamini, Y., Hochberg, Y., 1995. Controlling the false discovery rate: a pratical and powerful approch to multiple testing. R. Stat. Soc. 57, 289–300.

Bernasconi, F., Blondiaux, E., Potheegadoo, J., Stripeikyte, G., Pagonabarraga, J., Bejr-kasem, H., Bassolino, M., Akselrod, M., Martinez-horta, S., Sampedro, F., Hara, M., Horvath, J., Franza, M., Konik, S., Bereau, M., Ghika, J., Burkhard, P.R., Ville, D.V.D., Faivre, N., Rognini, G., Krack, P., 2021. Robot-induced hallucinations in Parkinson's disease depend on altered sensorimotor processing in fronto-temporal network. Sci. Transl. Med. 8362, 1–13.

Blakemore, S.J., Oakley, D.A., Frith, C.D., 2003. Delusions of alien control in the normal brain. Neuropsychologia 41, 1058–1067. doi:10.1016/S0028-3932(02)00313-5.

Blanke, O., 2012. Multisensory brain mechanisms of bodily self-consciousness. Nat. Rev. Neurosci. 13, 556–571. doi:10.1038/nrn3292.

Blanke, O., Arzy, S., Landis, T., 2008. Chapter 22 Illusory reduplications of the human body and self. Handb. Clin. Neurol. 88, 429–458. doi:10.1016/S0072-9752(07)88022-5.

Blanke, O., Ortigue, S., Coeytaux, A., Martory, M.D., Landis, T., 2003. Hearing of a presence. Neurocase 9, 329–339. doi:10.1076/neur.9.4.329.15552.

Blanke, O., Pozeg, P., Hara, M., Heydrich, L., Serino, A., Yamamoto, A., Higuchi, T., Salomon, R., Seeck, M., Landis, T., Arzy, S., Herbelin, B., Bleuler, H., Rognini, G., 2014. Neurological and robot-controlled induction of an apparition. Curr. Biol. 24, 2681–2686. doi:10.1016/j.cub.2014.09.049.

Bolton, T.A.W., Morgenroth, E., Preti, M.G., Van De Ville, D., 2020a. Tapping into multifaceted human behavior and psychopathology using fMRI brain dynamics. Trends Neurosci. 43, 667–680. doi:10.1016/j.tins.2020.06.005.

Bolton, T.A.W., Tarun, A., Sterpenich, V., Schwartz, S., Van De Ville, D., 2018. Interactions between large-scale functional brain networks are captured by sparse coupled HMMs. IEEE Trans. Med. Imaging 37, 230–240. doi:10.1109/TMI.2017.2755369.

Bolton, T.A.W., Tuleasca, C., Wotruba, D., Rey, G., Dhanis, H., Gauthier, B., Delavari, F., Morgenroth, E., Gaviria, J., Blondiaux, E., Smigielski, L., Van De Ville, D., 2020b. TbCAPs: a toolbox for co-activation pattern analysis. Neuroimage 211, 116621. doi:10.1016/j.neuroimage.2020.116621.

Bolton, T.A.W., Urunuela, E., Tian, Y., Zalesky, A., Caballero-Gaudes, C., Van De Ville, D., 2020c. Sparse coupled logistic regression to estimate co-activation and modulatory influences of brain regions. J. Neural Eng. 17. doi:10.1088/1741-2552/aba55e.

Brugger, P., Regard, M., Landis, T., 1997. Illusory reduplication of one's own body: phenomenology and classification of autoscopic phenomena. Cogn. Neuropsychiatry 2, 19–38. doi:10.1080/135468097396397.

Brugger, P., Regard, M., Landis, T., 1996. Unilaterally felt "presences": the neuropsychiatry of one's invisible doppelgänger. Neuropsychiatry Neuropsychol. Behav. Neurol. 9, 114–122.

Chen, J.E., Chang, C., Greicius, M.D., Glover, G.H., 2015. Introducing co-activation pattern metrics to quantify spontaneous brain network dynamics. Neuroimage 111, 476–488. doi:10.1016/j.neuroimage.2015.01.057.

Damaraju, E., Allen, E.A., Belger, A., Ford, J.M., McEwen, S., Mathalon, D.H., Mueller, B.A., Pearlson, G.D., Potkin, S.G., Preda, A., Turner, J.A., Vaidya, J.G., Van Erp, T.G., Calhoun, V.D., 2014. Dynamic functional connectivity analysis reveals transient states of dysconnectivity in schizophrenia. NeuroImage Clin. 5, 298–308. doi:10.1016/j.nicl.2014.07.003.

Diederich, N.J., Fénelon, G., Stebbins, G., Goetz, C.G., 2009. Hallucinations in Parkinson disease. Nat. Rev. Neurol. 5, 331–342. doi:10.1038/nrneurol.2009.62.

Ettinger, U., Mohr, C., Gooding, D.C., Cohen, A.S., Rapp, A., Haenschel, C., Park, S., 2015. Cognition and brain function in schizotypy: a selective review. Schizophr. Bull. 41, S417–S426. doi:10.1093/schbul/sbu190.

Farrer, C., Franck, N., Frith, C.D., Decety, J., Georgieff, N., D'Amato, T., Jeannerod, M., 2004. Neural correlates of action attribution in schizophrenia. Psychiatry Res. Neuroimaging 131, 31–44. doi:10.1016/j.pscychresns.2004.02.004.

Farrer, C., Frey, S.H., Van Horn, J.D., Tunik, E., Turk, D., Inati, S., Grafton, S.T., 2008. The angular gyrus computes action awareness representations. Cereb. Cortex 18, 254–261. doi:10.1093/cercor/bhm050.

Farrer, C., Frith, C.D., 2002. Experiencing oneself vs another person as being the cause of an action: the neural correlates of the experience of agency. Neuroimage 15, 596–603. doi:10.1006/nimg.2001.1009.

Fénelon, G., Soulas, T., De Langavant, L.C., Trinkler, I., Bachoud-Lévi, A.C., 2011. Feeling of presence in Parkinson's disease. J. Neurol. Neurosurg. Psychiatry 82, 1219–1224. doi:10.1136/jnnp.2010.234799.

Ferri, F., Frassinetti, F., Ardizzi, M., Costantini, M., Gallese, V., 2012. A sensorimotor network for the bodily self. J. Cogn. Neurosci. 24, 1584–1595. doi:10.1162/jocn_a_00230.

Ffytche, H.D., Creese, B., Politis, M., Chaudhuri, K.R., Weintraub, D., Ballard, C., Aarsland, D., 2017. The psychosis spectrum in Parkinson disease. Nat. Rev. Neurol. doi:10.1038/nrneurol.2016.200.

Fletcher, P.C., Frith, C.D., 2009. Perceiving is believing: a Bayesian approach to explaining the positive symptoms of schizophrenia. Nat. Rev. Neurosci. 10, 48–58. doi:10.1038/nrn2536.

Fox, M.D., Raichle, M.E., 2007. Spontaneous fluctuations in brain activity observed with functional magnetic resonance imaging. Nat. Rev. Neurosci. 8, 700–711. doi:10.1038/nrn2201.

Friston, K.J., 2011. Functional and effective connectivity: a review. Brain Connect 1, 13–36. doi:10.1089/brain.2011.0008.

Ghazanfar, A.A., Schroeder, C.E., 2006. Is neocortex essentially multisensory? Trends Cogn. Sci. 10, 278–285. doi:10.1016/j.tics.2006.04.008.

Goulden, N., Khusnulina, A., Davis, N.J., Bracewell, R.M., Bokde, A.L., McNulty, J.P., Mullins, P.G., 2014. The salience network is responsible for switching between the default mode network and the central executive network: replication from DCM. Neuroimage 99, 180–190. doi:10.1016/j.neuroimage.2014.05.052.

Gusnard, D.A., Akbudak, E., Shulman, G.L., Raichle, M.E., 2001. Medial prefrontal cortex and self-referential mental activity: relation to a default mode of brain function. Proc. Natl. Acad. Sci. USA 98, 4259–4264. doi:10.1073/pnas.071043098.

Hutchison, R.M., Womelsdorf, T., Allen, E.A., Bandettini, P.A., Calhoun, V.D., Corbetta, M., Della Penna, S., Duyn, J.H., Glover, G.H., Gonzalez-Castillo, J., Handwerker, D.A., Keilholz, S., Kiviniemi, V., Leopold, D.A., de Pasquale, F., Sporns, O., Walter, M., Chang, C., 2013. Dynamic functional connectivity: promise, issues, and interpretations. Neuroimage 80, 360–378. doi:10.1016/j.neuroimage.2013.05.079.

Ionta, S., Martuzzi, R., Salomon, R., Blanke, O., 2013. The brain network reflecting bodily self-consciousness: a functional connectivity study. Soc. Cogn. Affect. Neurosci. 9, 1904–1913. doi:10.1093/scan/nst185.

James, W., 1902. A Study of Man: The Varieties of Religious Experiences. Longmans, Green Co doi:10.1353/jsp.2003.0021.

Jardri, R., Thomas, P., Delmaire, C., Delion, P., Pins, D., 2013. The neurodynamic organization of modality-dependent hallucinations. Cereb. Cortex 23, 1108–1117. doi:10.1093/cercor/bhs082.

Jaspers, K., 1913. Über leibhafte Bewusstheiten (Bewusstheitstäuschugen), ein psychopathologisches Elementarsymptom. Z. Pathopsychol. 2, 150–161.

Kiviniemi, V., Vire, T., Remes, J., Elseoud, A.A., Starck, T., Tervonen, O., Nikkinen, J., 2011. A sliding time-window ICA reveals spatial variability of the default mode network in time. Brain Connect. 1, 339–347. doi:10.1089/brain.2011.0036.

Lefebvre, S., Demeulemeester, M., Leroy, A., Delmaire, C., Lopes, R., Pins, D., Thomas, P., Jardri, R., 2016. Network dynamics during the different stages of hallucinations in schizophrenia. Hum. Brain Mapp. 37, 2571–2586. doi:10.1002/hbm.23197.

Lenka, A., Pagonabarraga, J., Pal, P.K., Bejr-kasem, H., Kulisvesky, J., 2019. Minor hallucinations in Parkinson disease A subtle symptom with major clinical implications 1–9. 10.1212/WNL.0000000000007913

Liu, X., 2016. Chapter 3–Linear Mixed-Effects Models, in: Liu, X.B.T.-M. and A. of L.D.A. (Ed.), . Academic Press, Oxford, pp. 61–94. 10.1016/B978-0-12-801342-7.00003-4

Liu, X., Duyn, J.H., 2013. Time-varying functional network information extracted from brief instances of spontaneous brain activity. Proc. Natl. Acad. Sci. USA 110, 4392–4397. doi:10.1073/pnas.1216856110.

Liu, X., Zhang, N., Chang, C., Duyn, J.H., 2018. NeuroImage Co-activation patterns in resting-state fMRI signals. Neuroimage 180, 485–494. doi:10.1016/j.neuroimage.2018.01.041.

Manoliu, A., Riedl, V., Zherdin, A., Mühlau, M., Schwerthöffer, D., Scherr, M., Peters, H., Zimmer, C., Förstl, H., Bäuml, J., Wohlschläger, A.M., Sorg, C., 2014. Aberrant dependence of default mode/central executive network interactions on anterior insular salience network activity in schizophrenia. Schizophr. Bull. 40, 428–437. doi:10.1093/schbul/sbt037.

Matsuhashi, M., Ikeda, A., Ohara, S., Matsumoto, R., Yamamoto, J., Takayama, M., Satow, T., Begum, T., Usui, K., Nagamine, T., Mikuni, N., Takahashi, J., Miyamoto, S., Fukuyama, H., Shibasaki, H., 2004. Multisensory convergence at human temporoparietal junction - Epicortical recording of evoked responses. Clin. Neurophysiol. 115, 1145–1160. doi:10.1016/j.clinph.2003.12.009.

Menon, V., 2011. Large-scale brain networks and psychopathology: a unifying triple network model. Trends Cogn. Sci. 15, 483–506. doi:10.1016/j.tics.2011.08.003.

Menon, V., Uddin, L.Q., 2010. Saliency, switching, attention and control: a network model of insula function. Brain Struct. Funct. 214, 655–667. doi:10.1007/s00429-010-0262-0.

Messner, R., 2016. Naked Mountain: Nanga Parbat, Brother, Death, Solitude. Crowood.

Mlakar, J., Jensterle, J., Frith, C.D., 1994. Central monitoring deficiency. Psychol. Med. 24, 557–564.

Monti, S., Tamayo, P., Mesirov, J., Golub, T., 2003. Consensus clustering: a resampling-based method for class discovery and visualization of gene expression microarray data. Mach. Learn. 52, 91–118. doi:10.1023/A:1023949509487.

Oldfield, R.C., 1971. The assessment and analysis of handedness: the Edinburgh Inventory. Neuropsychologia 9, 97–113. doi:10.1007/978-0-387-79948-3_6053.

Platek, S.M., Loughead, J.W., Gur, R.C., Busch, S., Ruparel, K., Phend, N., Panyavin, I.S., Langleben, D.D., 2006. Neural substrates for functionally discriminating self-face from personally familiar faces. Hum. Brain Mapp. 27, 91–98. doi:10.1002/hbm.20168.

Power, J.D., Barnes, K.A., Snyder, A.Z., Schlaggar, B.L., Petersen, S.E., 2012. Spurious but systematic correlations in functional connectivity MRI networks arise from subject motion. Neuroimage 59, 2142–2154. doi:10.1016/j.neuroimage.2011.10.018.

Preti, M.G., Bolton, T.A., Van De Ville, D., 2017. The dynamic functional connectome: state-of-the-art and perspectives. Neuroimage 160, 41–54. doi:10.1016/j.neuroimage.2016.12.061.

Qin, P., Northoff, G., 2011. How is our self related to midline regions and the default-mode network? Neuroimage 57, 1221–1233. doi:10.1016/j.neuroimage.2011.05.028.

Raichle, M.E., MacLeod, A.M., Snyder, A., Powers, W.J., Gusnard, D.A., 2001. A default mode of brain function. Proc. Natl. Acad. Sci. 98, 676–682.

Rashid, B., Damaraju, E., Pearlson, G.D., Calhoun, V.D., 2014. Dynamic connectivity states estimated from resting fMRI Identify differences among Schizophrenia, bipolar disorder, and healthy control subjects. Front. Hum. Neurosci. 8, 1–13. doi:10.3389/fnhum.2014.00897.

Sahib, A.K., Erb, M., Marquetand, J., Martin, P., Elshahabi, A., Klamer, S., Vulliemoz, S., Scheffler, K., Ethofer, T., Focke, N.K., 2018. Evaluating the impact of fast-fMRI on dynamic functional connectivity in an event-based paradigm. PLoS One 13, 1–15. doi:10.1371/journal.pone.0190480.

Shine, J.M., Muller, A.J., O'Callaghan, C., Hornberger, M., Halliday, G.M., Lewis, S.J.G., 2015. Abnormal connectivity between the default mode and the visual system underlies the manifestation of visual hallucinations in Parkinson's disease: a task-based fMRI study. Parkinsons. Dis. 1. doi:10.1038/npjparkd.2015.3.

Shine, J.M., O'Callaghan, C., Halliday, G.M., Lewis, S.J.G., 2014. Tricks of the mind: visual hallucinations as disorders of attention. Prog. Neurobiol. 116, 58–65. doi:10.1016/j.pneurobio.2014.01.004.

Shirer, W.R., Ryali, S., Rykhlevskaia, E., Menon, V., Greicius, M.D., 2012. Decoding subject-driven cognitive states with whole-brain connectivity patterns. Cereb. Cortex 22, 158–165. doi:10.1093/cercor/bhr099.

Skudlarski, P., Jagannathan, K., Anderson, K., Stevens, M.C., Calhoun, V.D., Skudlarska, B.A., Pearlson, G., 2010. Brain connectivity is not only lower but different in schizophrenia: a combined anatomical and functional approach. Biol. Psychiatry 68, 61–69. doi:10.1016/j.biopsych.2010.03.035.

Sridharan, D., Levitin, D.J., Menon, V., 2008. A critical role for the right fronto-insular cortex in switching between central-executive and default-mode networks. Proc. Natl. Acad. Sci. USA 105, 12569–12574. doi:10.1073/pnas.0800005105.

Tagliazucchi, E., Balenzuela, P., Fraiman, D., Chialvo, D.R., 2012. Criticality in large-scale brain fmri dynamics unveiled by a novel point process analysis. Front. Physiol. 1–12. doi:10.3389/fphys.2012.00015.

Tagliazucchi, E., Balenzuela, P., Fraiman, D., Montoya, P., Chialvo, D.R., 2011. Spontaneous BOLD event triggered averages for estimating functional connectivity at resting state. Neurosci. Lett. 488, 158–163. doi:10.1016/j.neulet.2010.11.020.

Valdés-Sosa, P.A., Sánchez-Bornot, J.M., Lage-Castellanos, A., Vega-Hernández, M., Bosch-Bayard, J., Melie-García, L., Canales-Rodríguez, E., 2005. Estimating brain functional connectivity with sparse multivariate autoregression. Philos. Trans. R. Soc. B Biol. Sci. 360, 969–981. doi:10.1098/rstb.2005.1654.

Vidaurre, D., Smith, S.M., Woolrich, M.W., 2017. Brain network dynamics are hierarchically organized in time 114. 10.1073/pnas.1705120114

Whitfield-Gabrieli, S., Moran, J.M., Nieto-Castañón, A., Triantafyllou, C., Saxe, R., Gabrieli, J.D.E., 2011. Associations and dissociations between default and self-reference networks in the human brain. Neuroimage 55, 225–232. doi:10.1016/j.neuroimage.2010.11.048.

Zhang, G., Cai, B., Zhang, A., Stephen, J.M., Wilson, T.W., Calhoun, V.D., Wang, Y.P., 2020. Estimating dynamic functional brain connectivity with a sparse hidden markov model. IEEE Trans. Med. Imaging 39, 488–498. doi:10.1109/TMI.2019.2929959.

Zito, G.A., Wiest, R., Aybek, S., 2020. Neural correlates of sense of agency in motor control: a neuroimaging meta-analysis. PLoS One 15, 1–17. doi:10.1371/journal.pone.0234321.